Electronic Supplementary Material

Plate-height model of ion mobility-mass spectrometry

Márkó Grabarics[1,2]*, Maike Lettow[1,2], Ansgar T. Kirk[3], Gert von Helden[2], Tim J. Causon[4] and Kevin Pagel[1,2]*

1) Department of Biology, Chemistry and Pharmacy, Institute of Chemistry and Biochemistry, Freie Universität Berlin, Takustrasse 3, 14195 Berlin, Germany

2) Fritz Haber Institute of the Max Planck Society, Department of Molecular Physics, Faradayweg 4-6, 14195 Berlin, Germany

3) Institute of Electrical Engineering and Measurement Technology, Department of Sensors and Measurement Technology, Leibniz Universität Hannover, Appelstrasse 9A, 30167 Hannover, Germany

4) Department of Chemistry, Institute of Analytical Chemistry, University of Natural Resources and Life Sciences, Vienna, Muthgasse 18, 1190 Vienna, Austria

*Corresponding authors:

Email: grabarics@fhi-berlin.mpg.de

Email: kevin.pagel@fu-berlin.de

S1. Some reflections on the conditional and semi-empirical resolving power theory

Even though the conditional and semi-empirical resolving power models represent major steps in the development of the theory of ion mobility separations, it is important to realize and point out some of their shortcomings. These drawbacks stem from the fact that these models are built upon the application of full-width-at-half-maxima and the summation of w_h^2. In case of the conditional resolving power theory, it leads to the overestimation of the injection pulse-width's contribution, while in case of the semi-empirical model this approach gave rise to some confusion regarding the optimal value of the correction factors (most prominently that of β). In contrast to the two aforementioned theories, the plate-height model rests on the addition of variances. The pillar of plate-height models is a fundamental statistical law: when the individual dispersion processes act independently, the variances add linearly (variances corresponding to independent or uncorrelated random variables are additive)[1]. This theorem is true for variances, but does not hold generally for the square of full-width-at-half-maxima, implying the inherent problem of the conditional resolving power theory and every model that is based on the addition of w_h^2.

Let us illuminate this problem with the help of a simple example, considering the addition of two, completely identical rectangular distributions. Assume that the width of the uniform distributions at the base is unity and, consequently, $w_h^2 = 1$. The sum will be a symmetric, triangular function whose width at the baseline equals 2. Being an isosceles triangle, w_h and w_h^2 will be 1. Clearly, w_h^2 does not appear as an additive quantity, because the sum of the uniform distributions' w_h^2 does not equal the w_h^2 of their sum ($1 + 1 \neq 1$). Detailed, step-by-step solution of the above and other similar problems regarding the addition of various distributions can be found in statistics textbooks, and the reader is referred to them in case of further interest in the topic[2].

The only situation where w_h^2 values add linearly is when exclusively normal distributions are added together, because the sum will also be Gaussian. It was pointed out also by Revercomb and Mason in their classic paper[3]. In other words, the shape of the distribution and the relation between variance and w_h^2 is maintained upon convolution (unlike in the above example, where the sum of two uniform functions appears to be triangular, meaning that the aforementioned relation between σ^2 and w_h^2 necessarily changes). It is a consequence of the central limit theorem of statistics: the sum of independent random variables converges toward a Gaussian, where the mean and the variance of the resulting distribution is given as the sum of the means and the variances of the individual variables, respectively[2]. Although the overall peak shapes (the ATDs) converge toward a normal distribution in DTIM-MS, it does not mean that each and every dispersion process leads to Gaussian zone spreading. Indeed, the initial distribution of the ion packets is generally described as a rectangular function. As a consequence, the addition of w_h^2 values will lead to an overestimation of the contribution of processes associated with rectangular zone spreading.

Unlike in the conditional resolving power theory, the figures of merit in the plate-height model are derived from the variances either directly, such as in case of $HETP$ and N, or indirectly, as in case of R_p. Although traditionally not employed within the plate-height concept, resolving power is the preferred figure of merit in the IMS and IM-MS communities. To conform to this general practice, R_p was incorporated into the plate-height model of IM-MS, as explained in Section 1.1. Briefly, the resolving power limit corresponding to a given dispersion process that is characterized by a non-Gaussian distribution can be obtained by calculating the FWHM of a Gaussian that has the very same variance as the distribution in question, and then deriving the R_p limit from the full-width-at-half-maximum of this virtual Gaussian.

In other words, by employing Eq. 4 to calculate R_p from N, the definition of the latter being based on σ^2. This ensures that all figures of merit in the plate-height model are additive after being raised to the appropriate power – σ^2, $HETP$, $\frac{1}{N}$ and R_p^{-2}.

The above approach breaks down only if the overall peak shape (the ATD) ceases to be Gaussian. If very long injection pulses are applied, diffusion and other dispersion processes and random events in the drift cell might not be able to turn the initial rectangular distribution into a zone that is sufficiently close to a Gaussian. In such a case, approximating the ATD with a normal distribution would lead to errors in the determination of the separation efficiency. Thus, the distribution of ions should be obtained using error functions and often numerical methods[3,4]. The simple, general relation between variance and w_h^2 that exists for Gaussians could not be applied. The aforementioned relation would vary with changing peak shapes, making its determination laborious. Fortunately, such situations rarely arise in IM-MS under common operating conditions (see the relative contribution of the individual dispersion processes in Figure 2), and the Gaussian approximation can be used within satisfying accuracy.

S2. Diffusion

The spatial variance generated due to diffusional broadening is given as:

$$(S1)\ \sigma^2_{L;diff} = 2Dt_d$$

Here, D is the (longitudinal) diffusion coefficient of the ion, while t_d is the drift time, the time available for the ions to spread due to diffusion. Ion clouds move in the drift tube with a constant velocity that is proportional to the electric field strength (E_d), the proportionality factor being the mobility of the ion:

$$(S2)\ v_d = KE_d = \frac{KV_d}{L_d}$$

In Eq. S2 V_d is the drift voltage (the electric potential difference between the two ends of the drift tube) and L_d is the length of the drift cell. Thus, the drift time appears as:

$$(S3)\ t_d = \frac{L_d^2}{KV_d}$$

We mention here that in CZE, where the distance between the electrodes and the distance between the injection and detection region can be different, the fraction $\frac{V}{E}$ does not necessarily equal the product vt, complicating the corresponding equations. In comparison, the situation in DTIMS is rather simple, as the two distances are exactly the same – the length of the drift tube. Therefore, they do not need to be treated separately in Eq. S3. Combining Eq. S1 and S3 yields:

$$(S4)\ \sigma^2_{L;diff} = L_d^2 \frac{2D}{KV_d}$$

The Nernst-Townsend-Einstein relation links the mobility of an ion to its diffusion coefficient in the same medium (where T is the absolute temperature, q is the charge of the ionic species and k_B is the Boltzmann constant):

$$(S5)\ K = \frac{Dq}{k_B T}$$

With the help of Eq. S5 we can express diffusion-related variance for IMS in a more meaningful form:

$$(S6a)\ \sigma^2_{L;diff} = L_d^2 \frac{2D}{KV_d} = L_d^2 \frac{2k_B T}{qV_d} \qquad (S6b)\ \sigma^2_{t;diff} = t_d^2 \frac{2D}{KV_d} = t_d^2 \frac{2k_B T}{qV_d}$$

It needs to be emphasized that the two above quantities are not equal, neither regarding their numerical values, nor their units. Eq. S6a refers to a spatial quantity, while Eq. S6b expresses variance in the time domain. Based on the above expressions of variance, the diffusion limit of plate number and resolving power can be finally given:

$$(S7)\ N_{diff} = \frac{KV_d}{2D} = \frac{qV_d}{2k_B T}$$

$$(S8)\ R_{p;diff} = \left(\frac{KV_d}{16Dln2}\right)^{1/2} = \left(\frac{qV_d}{16k_B Tln2}\right)^{1/2}$$

S3. Coulomb repulsion

S3.1. Rate of expansion due to Coulombic forces

To account for space charge effects, let us consider a spherical cloud of ions expanding freely without having to overcome any kind of barrier, following the calculations of Tolmachev *et al*[5]. The driving force of this spatial dispersion is the force exerted by the electric field on the ions located at the edge of the ion cloud. This electric field is the result of the ions' own charge, and is given by Gauss's law for electrostatics, which relates the electric flux (the surface integral of the electric field) to the total charge enclosed in a closed surface. In case of a spherical ion packet, Gauss's law can be written in the following simple form due to symmetry reasons:

$$(S9)\ E_{Clmb} = \frac{Q}{A_{sphere}\varepsilon_0} = \frac{Q}{4\pi r^2 \varepsilon_0}$$

In Eq. S9 Q is the total charge enclosed by the surface of the spherical ion cloud (A_{sphere}) with a radius of r, and ε_0 is the vacuum permittivity (approximating the permittivity of the buffer gas in the mobility cell). As shown by Eq. S9, the electric field strength on the surface of the ion cloud is independent of the ion density distribution, as long as spherical symmetry is maintained. E_{Clmb} is merely the function of permittivity, the total charge and the area of the sphere this charge is confined into.

The speed of the ion cloud's radial expansion (v_{Clmb}) is given as:

$$(S10)\ v_{Clmb} = \frac{dr}{dt} = KE_{Clmb}$$

Substituting Eq. S9 into Eq. S10 results in a first-order differential equation:

$$(S11)\ \frac{dr}{dt} = K\frac{Q}{4\pi r^2 \varepsilon_0}$$

By solving Eq. S11 we obtain the following formula:

$$(S12)\ r(t) = \left(\frac{3KQ}{4\pi\varepsilon_0}(\Delta t + t_0)\right)^{1/3}$$

In Eq. S12 $r(t)$ is the total radius of the ion cloud, Δt is the time elapsed since the start of its Coulomb-driven expansion, *i.e.* the time since injection, whereas t_0 is the constant of integration. The latter can be calculated from the initial radius of the injected ion cloud:

$$(S13)\ t_0 = r_0^3\frac{4\pi\varepsilon_0}{3KQ}$$

Although Eq. S12 shows that dispersion due to Coulomb repulsion cannot be completely decoupled from the injection pulse-width (reflecting the role of charge-density rather than that of the total charge), for simplicity and in order to address each dispersion process independently, we only deal with Δt in the following calculations and assume t_0 to be zero. The role of the initial finite size of the ion cloud is addressed in detail in a separate chapter. The change of the radius due to space-charge effects in this case is expressed in the following explicit form:

$$(S14)\ \Delta r = \left(\frac{3KQ}{4\pi\varepsilon_0}\Delta t\right)^{1/3}$$

The next step is to relate spatial variance resulting from Coulomb-driven dispersion ($\sigma^2_{L;Clmb}$) to the total change in the radius or volume of the expanding ion cloud. Let us denote the total change in radius (Δr) and volume (ΔV) as r_{full} and V_{full}, respectively, when Δt equals t_d (the relation between the two being $V_{full} = \frac{4}{3}\pi r^3_{full}$). In the model employed herein – a freely extending ion packet that keeps its spherical symmetry – expansion along each spatial dimension is equal ($\Delta x = \Delta y = \Delta z = \Delta r$). It also means that the total variance is evenly distributed among the three spatial dimensions ($\sigma^2_x = \sigma^2_y = \sigma^2_z = \sigma^2_{L;Clmb}$). Thus, the spatial variance generated during the whole separation along the axis of the drift cell ($\sigma^2_{L;Clmb}$) will be directly proportional to r^2_{full} and to $V^{2/3}_{full}$, while the corresponding spatial width of the distribution ($2\sigma_{L;Clmb}$) will be proportional to r_{full} and $V^{1/3}_{full}$.

S3.2. Relating spatial variance to the size of the ion cloud: the case of the uniformly populated sphere

The previous section explored the expansion of ion clouds due to space charge effects, following the approach of Tolmachev and co-workers[5]. In the aforementioned excellent study, the authors employed these equations to derive the Coulomb limited resolving power in accordance with the formalism of the conditional resolving power theory, inheriting the drawbacks of this FWHM-based model. To obtain the appropriate figures of merit in the plate-height model, such as the Coulomb limited resolving power or theoretical plates, one has to find the variance that is generated by this dispersion process. Herein, we present a method employing statistical moment analysis to relate r^2_{full} to $\sigma^2_{L;Clmb}$, allowing for the incorporation of space charge effects into the plate-height model of IM-MS.

So far the only criterion regarding the spatial arrangement of ions was a spherical symmetry. However, to obtain the relation between r^2_{full} and $\sigma^2_{L;Clmb}$ a suitable constant is needed that reflects the distribution of ions within the cloud:

$$(S15)\ \sigma^2_{L;Clmb} = C_{Clmb}\ r^2_{full}$$

C_{Clmb} can be obtained from the probability density function (PDF) that describes the distribution of ions along the z-coordinate, corresponding to the axis of the mobility cell. Tolmachev *et al.* considered a uniformly populated sphere as a possible scenario, where the distance between neighboring ions is irrespective of their position within the cloud, *i.e.* the ion density is constant and does not change during the separation (this case must not be confused with a uniform, also called rectangular distribution)[5]. This case was chosen as a starting point for the calculations below to explore the issue highlighted in Eq. S15, although with the aim of obtaining the variance instead of the full-width-at-half-maximum of the distribution.

Let us consider an ion cloud that moves along the z-axis with constant velocity and generates a signal upon hitting the detector that is situated in the x,y-plane. The signal intensity is proportional to the number of ions hitting a detector per unit time. In case of a uniformly populated sphere, therefore, it is proportional to the area of the circle that is cut out from the sphere by the plane of the detector. The density function of the resulting distribution is given by the disk integral of the sphere:

$$(S16)\ \pi \int_{-r_{full}}^{+r_{full}} \left(r^2_{full} - z^2\right) dz = \frac{4}{3}\pi r^3_{full}$$

In the above expression z is the distance between the center of the sphere and the plane of the detector along the axis of the drift cell (the axis being perpendicular to the plane of the detector).

The integral equals the volume of the sphere with a radius of r_{full}, in accordance with the fact that the area should be proportional to the total number of ions within the cloud. The probability density function (PDF) can be obtained upon normalization of the density function (Eq. S16):

$$(S17)\ A\pi \int_{-r_{full}}^{+r_{full}} \left(r_{full}^2 - z^2\right) dz = 1$$

The normalizing constant A appears as:

$$(S18)\ A = \frac{3}{4\pi r_{full}^3}$$

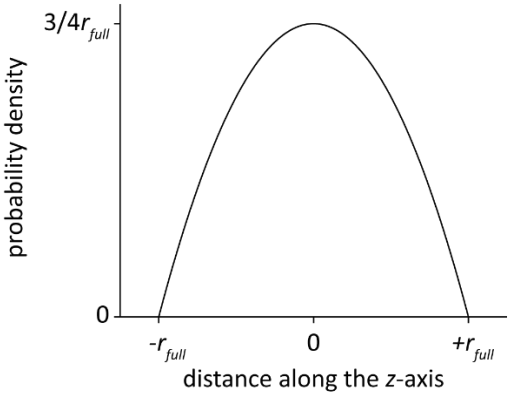

Figure S1. Graphical representation of the quadratic probability density function corresponding to a uniformly populated sphere with a radius of r_{full}.

Since the above quadratic distribution is symmetric with respect to the mean, the central moment of first order (the expected value, μ, not to be confused with the reduced mass) is zero:

$$(S19)\ \mu = A\pi \int_{-r_{full}}^{+r_{full}} z\left(r_{full}^2 - z^2\right) dz = 0$$

Therefore, the variance (central moment of second order) can be calculated as:

$$(S20)\ \sigma_{L;Clmb}^2 = A\pi \int_{-r_{full}}^{+r_{full}} z^2\left(r_{full}^2 - z^2\right) dz = \frac{r_{full}^2}{5}$$

The above equation (together with Eq. S15) shows that C_{Clmb} in case of a uniformly populated sphere (quadratic distribution) equals $\frac{1}{5}$.

Tolmachev *et al.* considered the very same quadratic probability density function (Eq. S17 and Figure S1). Instead of calculating the variance, however, the full-width-at-half-maximum (FWHM) of the quadratic distribution was used to obtain a proportionality factor[5]. This factor (termed C_S, keeping the original notation to make clear distinction from C_{Clmb}) was defined as the ratio between the FWHM of the density function and its width at the baseline (the diameter of the sphere). For a uniformly populated sphere C_S appeared to be $\frac{1}{\sqrt{2}}$. The FWHM value obtained by this approach was used to calculate the Coulomb limit of resolving power.

S3.3. Relating spatial variance to the size of the ion cloud: the case of arbitrary ion distributions

In the previous section statistical moment analysis was employed to obtain a factor that relates $\sigma^2_{L;Clmb}$ to the size of the ion cloud, considering a uniformly populated sphere. However, the uniform radial distribution of ions inside the sphere – resulting in the quadratic functions of Eq. S16 and Eq. S17 – is only one of the many potential scenarios. One can imagine situations where the distance between the ions within the sphere and the radial distribution function is not constant. Besides varying in space, the distribution of ions also changes in time, complicating the description of space charge effects.

The initial distribution of ions at the beginning of the ion mobility separation is generally associated with a rectangular function. This rectangular distribution will evolve in the course of the separation not only due to diffusion, but also due to the mutual repulsion between ions. Although thermal energies exceed those associated with the space charge under conditions that are typical in IMS and IM-MS, Coulombic forces still have some influence[6]. In the plate-height model it is assumed for the sake of simplicity that diffusion and Coulombic forces act independently. Let us realize that $\sigma^2_{L;Clmb}$ is based on multiple estimations: the number of charges is not determined accurately in everyday measurements and the ion clouds do not have perfect spherical symmetry. Thus, modelling the evolution of the ions' radial distribution during ion mobility separations due to space charge effects would bring little gain in the accuracy of calculating the suitable variances within this model. Therefore, we may consider different, realistic and justifiable distributions and calculate the corresponding C_{Clmb} without introducing significant errors. In case of a rectangular (continuous uniform) distribution, C_{Clmb} is equal to $\frac{1}{3}$, while for a Gaussian distribution C_{Clmb} appears as $\frac{1}{4}$. In the present study a rectangular distribution is considered for all calculations, in accordance with the initial rectangular distribution of the ion packet (keeping in mind that it will actually change in the course of the separation).

Although finding a suitable factor that relates $\sigma^2_{L;Clmb}$ to r^2_{full} is important, the rate of expansion of ion clouds is irrespective of the ions' distribution within the ion cloud (as mentioned before in relation to Eq. S13 and Eq. S14). Therefore, the most essential and practically relevant findings related to Coulomb-driven dispersion – such as N_{Clmb} and $R_{p;Clmb}$ being independent of the absolute values of transport properties – are unaffected by the actual value of C_{Clmb}.

S3.4. Coulomb limit of theoretical plates and resolving power

By combining Eq. S14 and S15, spatial and temporal variance generated during the whole separation ($\Delta t = t_d$) can be given in the following explicit forms:

$$(S21a)\ \sigma^2_{L;Clmb} = C_{Clmb}\left(\frac{3KQ}{4\pi\varepsilon_0}t_d\right)^{2/3} = C_{Clmb}\left(\frac{3Q}{4\pi\varepsilon_0 V_d}L_d^2\right)^{2/3}$$

$$(S21b)\ \sigma^2_{t;Clmb} = C_{Clmb}\left(\frac{3Q}{4\pi\varepsilon_0 V_d L_d}\right)^{2/3} t_d^2 = C_{Clmb}\left(\frac{3Q}{4\pi\varepsilon_0 V_d K E_d}t_d^2\right)^{2/3}$$

Based on the above expressions of variances, the Coulomb- or space charge limit of theoretical plates and resolving power can be formulated, analogously to Eq. S7 and Eq. S8 for diffusion:

$$(S22)\ N_{Clmb} = \frac{1}{C_{Clmb}}\left(\frac{4\pi\varepsilon_0 V_d}{3Q}L_d\right)^{2/3}$$

$$(S23)\ R_{p;Clmb} = \left(\frac{1}{C_{Clmb}\ 8ln2}\right)^{1/2}\left(\frac{4\pi\varepsilon_0 V_d}{3Q}L_d\right)^{1/3}$$

In summary, the effects of Coulomb forces on the resolving power of IMS were addressed above in accordance with the method of Tolmachev *et al.* (apart from calculating the value of C_{Clmb}), who presented one of the most thorough and comprehensive studies on the subject[5]. This model is based on the unrestricted, free expansion of spherical on clouds. Therefore, spatial variance due to Coulomb repulsion along all three spatial dimensions is equal and directly proportional to $\Delta V^{2/3}$ (ΔV being the change in the volume of the cloud due to Coulombic forces, not to be confused with the drift voltage). Several similar approaches – based on Gauss's law for electrostatics – can be found in the literature. Xu *et al.* considered a different geometry, their model being based on a cylindrical ion cloud[7]. Although the cylinder considered in this study had a finite length (comparable to its diameter), the common mathematical solution of Gauss's law for cylindrical shapes holds for infinitely long objects. Consequently, the length of the cylindrical ion cloud is fixed in the aforementioned study, meaning that it only expands radially. In other words, the total volume (or variance) generated due to Coulomb repulsion is distributed unevenly among the three spatial dimensions. The variance associated with Coulomb repulsion is zero along the axis parallel to the length of the cylinder, while it is systematically larger along the two remaining axes than in the spherical model presented here. It means that the equation $\sigma_x^2 = \sigma_y^2 = \sigma_z^2$ breaks down. Consequently, the Coulomb limit of resolving power appears to be proportional to $V_d^{1/2}$ and to $Q^{-1/2}$ (instead of to $V_d^{1/3}$ and to $Q^{-1/3}$), because the spatial variance along the *z*-coordinate is directly proportional to ΔV and not to $\Delta V^{2/3}$. Furthermore, the dimensionless constants are different as well, reflecting a cylindrical geometry instead of a spherical one. Kirk *et al.* also developed a method to estimate the effect of Coulombic forces on the resolving power of ion mobility spectrometers. They approximated the shape of the ion cloud in atmospheric pressure IMS by an infinitesimally thin disk and solved Gauss's law for the aforementioned geometry[8]. This approximation may hold when extremely short injection pulses are being applied.

S4. Exploring the plate-height equation in detail

S4.1 Plate-height equation for stand-alone IMS

As mentioned in Section 4.1, Eqs. 35-37 simplify significantly when only one compartment is considered, such as in stand-alone IMS. In this case $HETP_{IMS}$ appears as:

$$(S21)\ HETP_{IMS} = \frac{L_d}{N_{IMS}} = \frac{\sigma_L^2}{L_d} = \frac{\boldsymbol{B}V_d^2}{L_d} + \frac{\boldsymbol{C}}{L_d V_d^{2/3}} + \frac{\boldsymbol{D}}{L_d V_d}$$

$$\boldsymbol{B} = \frac{1}{C_{inj}}\left(\frac{Kt_{inj}}{L_d}\right)^2 \qquad \boldsymbol{C} = C_{Clmb}\left(\frac{3Q}{4\pi\varepsilon_0}L_d^2\theta\right)^{2/3} \qquad \boldsymbol{D} = L_d^2\frac{2k_BT}{q}\theta$$

Since only one compartment is present, there is no need for velocity correction. N_{IMS} can be calculated accordingly:

$$(S22)\ N_{IMS} = \frac{L_d^2}{\sigma_L^2} = \frac{L_d}{HETP_{IMS}} = \frac{L_d^2}{\boldsymbol{B}V_d^2 + \frac{\boldsymbol{C}}{V_d^{2/3}} + \frac{\boldsymbol{D}}{V_d}}$$

$R_{p;IMS}$ is given by definition as:

$$(S23)\ R_{p;IMS} = \left(\frac{N_{IMS}}{8ln2}\right)^{1/2} = (8ln2)^{-1/2}\frac{L_d}{\left(\boldsymbol{B}V_d^2 + \frac{\boldsymbol{C}}{V_d^{2/3}} + \frac{\boldsymbol{D}}{V_d}\right)^{\mathbf{1/2}}}$$

S4.2 Finding the minimum of the plate-height function

Let us neglect Coulomb repulsion and consider only diffusion and the width of the injected ion packet (as done in the majority of studies in the field):

$$(S24)\ HETP_{IMS} = \frac{\sigma_L^2}{L_d} = \frac{\boldsymbol{B}V_d^2 + \frac{\boldsymbol{D}}{V_d}}{L_d}$$

The derivative $dHETP_{IMS}/dV_d$ is zero where Eq. S24 has its minimum, *i.e.* where V_d equals $V_{d;opt}$:

$$(S25)\ \frac{dHETP_{IMS}}{dV_d} = \frac{2\boldsymbol{B}V_d - \frac{\boldsymbol{D}}{V_d^2}}{L_d}$$

$$(S26)\ \frac{2\boldsymbol{B}V_{d;opt} - \frac{\boldsymbol{D}}{V_{d;opt}^2}}{L_d} = 0$$

From Eq. S26 a very simple expression can be derived for $V_{d;opt}$:

$$(S27)\ V_{d;opt} = \left(\frac{\boldsymbol{D}}{2\boldsymbol{B}}\right)^{1/3}$$

By substituting Eq. S27 into Eq. 24 we can calculate $HETP_{IMS;opt}$:

$$(S28)\ HETP_{IMS;opt} = \frac{3}{L_d}\left(\frac{\boldsymbol{D}^2\boldsymbol{B}}{4}\right)^{1/3}$$

Analogously, the number of theoretical plates and resolving power at the optimal voltage appear as:

$$(S29)\ N_{IMS;opt} = \frac{L_d}{HETP_{IMS;opt}} = \frac{L_d^2}{3}\left(\frac{4}{\boldsymbol{D}^2\boldsymbol{B}}\right)^{1/3}$$

$$(S30)\ R_{p;IMS;opt} = \left(\frac{N_{IMS;opt}}{8ln2}\right)^{1/2} = \frac{L_d}{\sqrt{24ln2}}\left(\frac{2}{\boldsymbol{D}\sqrt{\boldsymbol{B}}}\right)^{1/3}$$

S4.3 Expressing $HETP_{app}$, N_{app} and $R_{p;app}$ with temporal variances

The total temporal variance in DTIM-MS appears as:

$$(S31)\ \sigma_{t;total}^2 = \boldsymbol{A_t} + \boldsymbol{B_t} + \frac{\boldsymbol{C_t}}{V_d^{2/3}} + \frac{\boldsymbol{D_t}}{V_d}$$

$$\boldsymbol{A_t} = 2D\frac{t_{fun}^2}{KV_{fun}} + C_{Clmb}\left(\frac{3Q}{4\pi\varepsilon_0 V_{fun}KE_{fun}}t_{fun}^2\right)^{2/3} \qquad \boldsymbol{B_t} = \frac{t_{inj}^2}{C_{inj}}$$

$$\boldsymbol{C_t} = C_{Clmb}\left(\frac{3Q}{4\pi\varepsilon_0 L_d}\right)^{2/3} t_d^2 \qquad \boldsymbol{D_t} = t_d^2\frac{2k_BT}{q}\theta$$

Let us realize that the temporal variance associated with the injection pulse-width and the post-cell region are completely independent of the drift voltage. Based on the expression above, the equivalents of Eqs. 35-37 using $\sigma_{t;total}^2$ can be formulated as follows:

$$(S32)\ HETP_{app} = L_{total}\frac{\sigma_{t;total}^2}{t_a^2}\left(\frac{1}{1-F}\right)^2 = \left(L_d + L_{fun}\right)\frac{\boldsymbol{A_t} + \boldsymbol{B_t} + \frac{\boldsymbol{C_t}}{V_d^{2/3}} + \frac{\boldsymbol{D_t}}{V_d}}{\left(t_d + t_{fun}\right)^2}$$

$$(S33)\ N_{app} = \frac{t_a^2}{\sigma_{t;total}^2}(1-F)^2 = \frac{\left(t_d + t_{fun}\right)^2}{\boldsymbol{A_t} + \boldsymbol{B_t} + \frac{\boldsymbol{C_t}}{V_d^{2/3}} + \frac{\boldsymbol{D_t}}{V_d}}$$

$$(S34)\ R_{p;app} = \left(\frac{N_{app}}{8ln2}\right)^{1/2} = (8ln2)^{-1/2}\frac{t_d + t_{fun}}{\left(\boldsymbol{A_t} + \boldsymbol{B_t} + \frac{\boldsymbol{C_t}}{V_d^{2/3}} + \frac{\boldsymbol{D_t}}{V_d}\right)^{1/2}}$$

It is important to mention that t_d – present in the terms $\boldsymbol{C_t}$ and $\boldsymbol{D_t}$, as well as in the denominator of S32 and the numerator of Eq. S33 and Eq. S34 – depends on the drift voltage.

S5. Experiment vs. theory

The equivalent of Figure 3 in Section 4.2 is shown below, depicting plate height instead of resolving power as a function of the drift voltage:

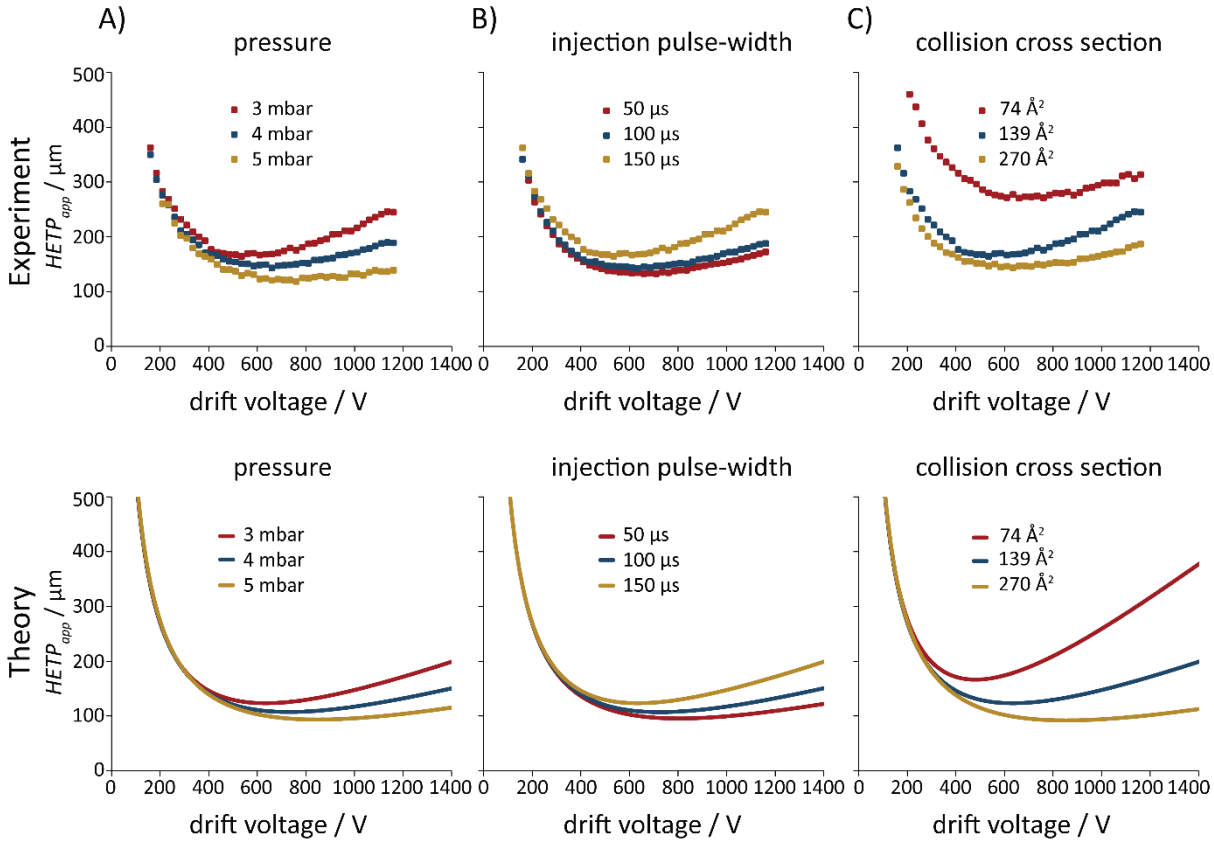

Figure S2. Plate height in IM-MS – experiment vs. theory. The equivalent of Figure 3, depicting plate height instead of resolving power. The effect of A) the buffer gas pressure, B) the injection pulse-width and C) the collision cross section of the ions on the apparent effective plate height ($HETP_{app}$) is highlighted. Experiments were performed in positive ion mode on a custom-built DTIM-MS instrument (L_d = 805.5 mm, L_{fun} = 144 mm) with He as buffer gas at ambient temperature (T = 295.0 ± 0.2 K). The following measurement conditions were used as a starting point with the corresponding curve presented in every graph (red, yellow and blue trace in A, B and C, respectively): p = 3 mbar, t_{inj} = 150 µs and ${}^{DT}\Omega_{He}$ = 139 Å^2 (trisaccharide Na^+ adduct). Each of the three aforementioned experimental parameters was varied systematically as follows. A) Buffer gas pressure varied in three steps: 3 mbar, 4 mbar and 5 mbar. B) Injection pulse-width varied in three steps: 50 µs, 100 µs and 150 µs. C) Collision cross section (influencing the mobility of the ions) varied in three steps: ${}^{DT}\Omega_{He}$ = 74 Å^2 (protonated 12-crown-4), 139 Å^2 (trisaccharide Na^+ adduct) and 270 Å^2 (TBAI trimer). Calculations were performed according to Eq. 35, considering a rectangular injection profile (C_{inj} = 12), ion clouds with a charge of Q = 100 000 e (C_{Clmb} = $\frac{1}{3}$, continuous uniform distribution) and a completely homogeneous electric field (θ = 1).

An additional set of experiments – similar to that imaged in Figure 3 and Figure S2 – was performed to test the plate-height model. The tetrabutylammonium iodide trimer cation served as the central species for the comparative analysis displayed below:

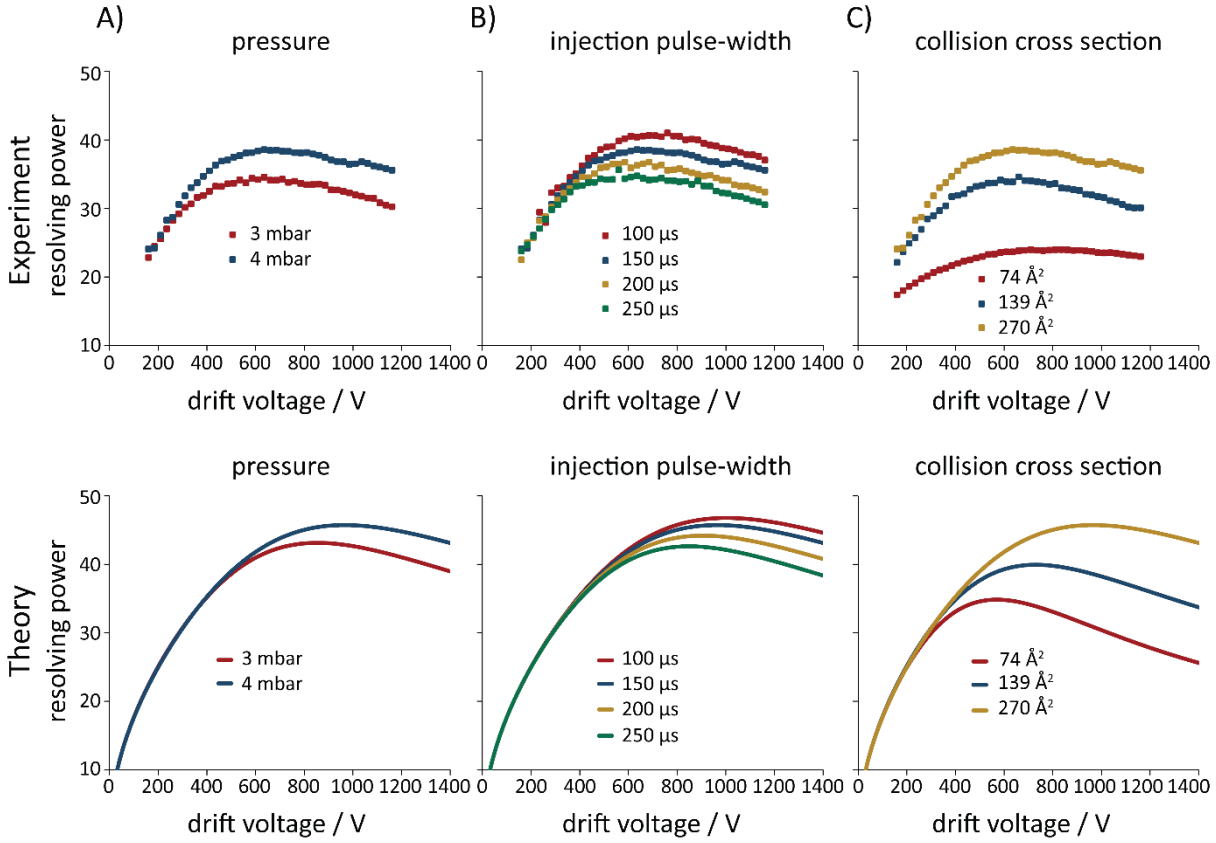

Figure S3. Experiment vs. theory – Part II. The effect of A) the buffer gas pressure, B) the injection pulse-width and C) the collision cross section of the ions on the apparent effective resolving power ($R_{p;app}$) is highlighted. Experiments were performed in positive ion mode on a custom-built DTIM-MS instrument (L_d = 805.5 mm, L_{fun} = 144 mm) with He as buffer gas at ambient temperature (T = 295.0 ± 0.2 K). The following measurement conditions were used as a starting point with the corresponding curve presented in every graph (blue, blue and yellow trace in A, B and C, respectively): p = 4 mbar, t_{inj} = 150 µs and ${}^{DT}\Omega_{He}$ = 270 Å² (TBAI trimer cation $[(TBA)_3I_2]^+$). Each of the three aforementioned experimental parameters was varied systematically as follows. A) Buffer gas pressure varied in two steps: 3 mbar and 4 mbar. B) Injection pulse-width varied in four steps: 100 µs, 150 µs, 200 µs and 250 µs. C) Collision cross section (influencing the mobility of the ions) varied in three steps: ${}^{DT}\Omega_{He}$ = 74 Å² (protonated 12-crown-4), 139 Å² (trisaccharide Na^+ adduct) and 270 Å² (TBAI trimer). Calculations were performed according to Eq. 37, considering a rectangular injection profile (C_{inj} = 12), ion clouds with a charge of Q = 100 000 e ($C_{Clmb} = \frac{1}{3}$, continuous uniform distribution) and a completely homogeneous electric field (θ = 1).

The plate-height model is again capable of reproducing experimental results with satisfying accuracy, which provides further validation of the underlying theory.

S6. Linear drift tube ion mobility separations in a spreadsheet

To facilitate the straightforward test and utilization of the plate-height model, we provide a spreadsheet template in a widely accessible and transparent file format. The spreadsheet may be used as provided to calculate the achievable N, $HETP$ and R_p in ion mobility separations after choosing appropriate input parameters specific for the researcher's experimental setup, or serve as the basis for writing more convenient programs for the same purpose. The spreadsheet is provided as part of the Electronic Supplementary Material.

References:

1 J. C. Giddings, *Unified Separation Science*, John Wiley & Sons, Inc., New York, 1991.

2 M. Bonamente, *Statistics and Analysis of Scientific Data*, Springer, New York, 2nd edn., 2017.

3 H. E. Revercomb and E. A. Mason, *Anal. Chem.*, 1975, **47**, 970–983.

4 X. Huang, W. F. Coleman and R. N. Zare, *J. Chromatogr. A*, 1989, **480**, 95–110.

5 A. V Tolmachev, B. H. Clowers, M. E. Belov and R. D. Smith, *Anal. Chem.*, 2009, **81**, 4778–4787.

6 M. Levin, A. Krisilov, B. Zon and G. Eiceman, *Int. J. Ion Mobil. Spectrom.*, 2014, **17**, 73–77.

7 J. Xu, W. B. Whitten and J. M. Ramsey, *Anal. Chem.*, 2000, **72**, 5787–5791.

8 A. T. Kirk, M. Allers, P. Cochems, J. Langejuergen and S. Zimmermann, *Analyst*, 2013, **138**, 5200–5207.